Published in final edited form as:
NMR Biomed. 2023 August ; 36(8): e4923. doi:10.1002/nbm.4923.

A Single Breath-hold Protocol for Hyperpolarized ^{129}Xe Ventilation and Gas Exchange Imaging

Peter J. Niedbalski[1,2,3,*], **Matthew M. Willmering**[4], **Robert P. Thomen**[5], **John P. Mugler III**[6], **Jiwoong Choi**[1,2], **Chase Hall**[1], **Mario Castro**[1]

[1]Division of Pulmonary, Critical Care, and Sleep Medicine, Department of Internal Medicine, University of Kansas Medical Center, Kansas City, KS, USA

[2]Department of Bioengineering, University of Kansas, Lawrence, KS, USA

[3]Hoglund Biomedical Imaging Center, University of Kansas Medical Center, Kansas City, KS, USA

[4]Center for Pulmonary Imaging Research, Cincinnati Children's Hospital Medical Center, Cincinnati, OH, USA

[5]Departments of Radiology and Bioengineering, University of Missouri School of Medicine, Columbia, MO, USA

[6]Department of Radiology & Medical Imaging, University of Virginia School of Medicine, Charlottesville, VA, USA

Abstract

Hyperpolarized ^{129}Xe MRI (Xe-MRI) is increasingly used to image the structure and function of the lungs. Because ^{129}Xe imaging can provide multiple contrasts (ventilation, alveolar airspace size, and gas exchange), imaging often occurs over several breath-holds, which increases the time, expense, and patient burden of scans. We propose an imaging sequence that can be used to acquire Xe-MRI gas exchange and high-quality ventilation images within a single, ~10 s breath-hold. This method uses a radial 1-point Dixon approach to sample dissolved ^{129}Xe signal, which is interleaved with a 3D spiral ("FLORET") encoding pattern for gaseous ^{129}Xe. Thus, ventilation images are obtained at higher nominal spatial resolution (4.2 x 4.2 x 4.2 mm^3) compared to gas-exchange images (6.25 x 6.25 x 6.25 mm^3), both competitive with current standards within the Xe-MRI field. Moreover, the short 10 s Xe-MRI acquisition time allows for ^{1}H "anatomic" images used for thoracic cavity masking to be acquired within the same breath-hold for a total scan time of ~14 s. Images were acquired using this single-breath method in 11 volunteers (N = 4 healthy, N = 7 post-acute COVID). For 11 of these subjects, a separate breath-hold was used to acquire a "dedicated" ventilation scan and 5 had an additional "dedicated" gas exchange scan. The images acquired using the single-breath protocol were compared to those from dedicated scans using Bland-Altman analysis, intra-class correlation (ICC), structural similarity, peak SNR (PSNR), Dice coefficients, and average distance. Imaging markers from the single-breath protocol showed high correlation with dedicated scans (Ventilation Defect Percent, ICC = 0.77, $p = 0.01$, membrane/gas, ICC = 0.97, $p = 0.001$, and red blood cell/gas, ICC = 0.99, $p < 0.001$). Images

---

[*]Corresponding Author: Peter J. Niedbalski, 3901 Rainbow Blvd, Mail Stop 3007, Kansas City, KS 66160, pniedbalski@kumc.edu.

showed good qualitative and quantitative regional agreement. This single-breath protocol enables the collection of essential Xe-MRI information within one breath-hold, simplifying scanning sessions and reducing costs associated with Xe-MRI.

Keywords

Hyperpolarized ^{129}Xe; Ventilation; Gas Exchange; Spiral; Dixon

INTRODUCTION

Hyperpolarized ^{129}Xe MRI (Xe-MRI) is increasingly being considered as a modality for understanding the structure and function of the lungs.[1,2] Xe-MRI typically provides 3 main contrasts: ventilation, alveolar airspace size (from measurement of gas diffusion), and gas exchange.[2] One of the challenges of performing Xe-MRI, particularly in patients with severe lung disease, is the requirement of several long breath-holds to encode images with these different contrasts. For example, the current recommended protocols require breath-holds of ~10 s (ventilation), 16 s (alveolar airspace size), and 15 s (gas exchange).[2] While there are novel techniques in place at various research institutions for more rapid imaging,[3-10] there typically remains the requirement of distinct breath-holds for imaging each contrast.

For both alveolar airspace size and gas exchange imaging, low-resolution ventilation images are acquired alongside the diffusion-weighted (alveolar airspace size) or dissolved-phase images (gas exchange).[11-15] While these ventilation images are essential for accurate quantification,[16,17] they are often considered to have spatial resolution that is too low to be of diagnostic quality for assessing ventilation itself. As such, even for scanning sessions in which one or both of alveolar airspace size and gas exchange imaging is performed, a separate breath-hold for ventilation imaging is typically required.

Innovations in rapid imaging of hyperpolarized ^{129}Xe present a means by which high quality ventilation images can be acquired simultaneously with diffusion or gas exchange images. Specifically, 3D spiral and/or compressed sensing acquisition can be used for rapid acquisition of 3D ventilation images with high resolution (in comparison to slice selective imaging methods).[6],[7] Moreover, flip angle/TR equivalence has enabled flexibility in the timing and breath-hold duration of gas exchange imaging.[18,19] Herein, we present our strategy for combining high resolution 3D ventilation imaging with the 1-point Dixon technique of gas exchange imaging, thereby reducing the Xe-MRI session to a single breath-hold when both gas-exchange and high-quality ventilation images are required.

MATERIAL AND METHODS

Subjects

All human studies were approved by the University of Kansas Medical Center Institutional Review Board. All research participants provided written informed consent prior to participation in this study.

We imaged a total of 11 subjects: 4 Healthy (3F/1M, age 42 ± 19) and 7 post-acute COVID-19 (6F/1M, age 43 ± 15). Post-acute COVID-19 participants all had long term COVID-19 symptoms broadly defined as any persistent symptoms, unexplained by another cause, at the time of MRI (>3-months post-acute infection). All post-acute COVID-19 participants had mild/moderate COVID-19 not requiring hospitalization.

Gas Polarization and Delivery

Isotopically enriched (90% ^{129}Xe) xenon gas (Nukem Isotopes GmbH, Alzenau, Germany) was polarized to ~30% using a Polarean 9820 xenon hyperpolarizer (Polarean Imaging Plc., Durham, NC). The total dose volume delivered to subjects was equal to 20% of each subject's estimated forced vital capacity from the prediction tool of the Global Lung Function Initiative (http://gli-calculator.ersnet.org/index.html). Because ventilation imaging requires less signal intensity to generate high quality images, doses delivered for ventilation imaging contained 70% hyperpolarized xenon with the balance ultra-high purity N_2. Doses delivered for gas exchange imaging contained 100% hyperpolarized xenon. Subjects inhaled xenon doses from approximate functional residual capacity. To assist with comparisons between images acquired with different xenon volumes and polarization levels, the dose equivalent volume (DEV) was calculated for each dose.[20]

All subjects were imaged using a 3T Skyra MRI scanner (Siemens, Erlangen, Germany) using a flexible transmit/receive ^{129}Xe vest coil (Clinical MR Solutions, LLC, Brookfield, WI). Prior to imaging, xenon resonance frequency, transmitter power, RBC/membrane ratio, and TE90 (echo time at which RBC and Membrane are 90° out of phase) were calibrated using a calibration protocol recommended by the ^{129}Xe MRI Clinical Trials Consortium.[2] Calibration data was analyzed in real-time using a home-built MATLAB (version 2020A, MathWorks, Natick MA) program, which can be found here: https://github.com/pniedbalski3/Calibration_App. Following this, every subject was imaged by a 3D spiral imaging sequence for ventilation imaging and a single-breath ventilation/gas-exchange sequence. N = 5 subjects (2 healthy, 3 post-COVID-19) were additionally imaged using a dedicated gas-exchange sequence following our previously published protocol.[19] After xenon imaging, a geometry-matched ^{1}H anatomic image set was acquired within the same breath-hold for each imaging type.

Finally, we imaged 1 healthy participant using the single-breath acquisition twice about 10 minutes apart to generate a preliminary assessment of scan-to-scan repeatability.

Dedicated Spiral Ventilation

Herein, ventilation images acquired during a separate breath-hold are referred to as "dedicated ventilation." Dedicated ventilation images were acquired using the FLORET 3D spiral sampling scheme.[7,21,22] The imaging sequence was created in-house using spiral gradient calculations described by Pipe et al.[21,23,24] Parameters for dedicated ventilation imaging are shown in Table 1.

Dedicated Gas Exchange

Herein, gas exchange images acquired during a separate breath-hold using the 1-point Dixon method, as described previously,[19] are referred to as “dedicated gas exchange.” Dedicated gas exchange images were acquired using a 3D radial 1-point Dixon technique. As we have previously reported,[19] flip angle and TR were reduced such that $TR_{90,equiv}$ = 249 ms,[18] the value associated with parameters recommended by the ^{129}Xe MRI Clinical Trials Consortium. Prior to data acquisition, 30 dummy pulses (using a maximum possible flip angle of 25°) were applied at the dissolved phase frequency to deplete magnetization downstream of the pulmonary microvasculature. Parameters for dedicated gas exchange imaging are shown in Table 1.

Single-Breath Ventilation/Gas Exchange

While traditional chemical shift imaging (CSI) methods have been employed for Xe-MRI gas exchange imaging, accelerated spectroscopic imaging techniques, such as 1-point[12] and multi-point Dixon[14,25] imaging, are most commonly used. In these techniques, imaging of the dissolved phase is interleaved with imaging of the gas phase. To date, most implementations have used the same encoding scheme for both the gas and dissolved acquisition. For example, the commonly used 1-point Dixon technique uses a 3D radial acquisition at the dissolved frequency interleaved with a 3D radial acquisition at the gas frequency. Radial imaging is commonly used to acquire dissolved xenon signal, because T_2^* of the dissolved components is very short (~1 ms at 3T). However, gaseous xenon does not suffer from this fast relaxation (T_2^* ~18 ms at 3T), and thus radial acquisition inefficiently samples the available magnetization.

To make use of the long duration of signal from gaseous xenon, we use a 3D spiral (FLORET)[7,21,22] acquisition to collect images at the gas frequency, which is interleaved with a 3D radial acquisition for dissolved images. While spiral acquisition could, in principle, be used for dissolved acquisition as well, the short T_2^* of dissolved signal significantly reduces the possible duration of spiral sampling. Over the short imaging window afforded by imaging during a breath-hold, the efficiency gains of spiral acquisition of the dissolved phase would be marginal. As such, we opted to retain radial sampling for the dissolved phase. The total time (including excitation, spoiling, etc.) per interleaf for dissolved (radial) sampling is 2.7 ms, while that for gaseous (spiral) sampling is 5.3 ms. Gradient spoiling is performed along the x-axis following the ^{129}Xe MRI Clinical Trials Consortium recommendations.[2] For Xe-MRI gas exchange imaging, the contrast of images depends on the time between acquisitions at like-frequencies – i.e., the time from one RF pulse at the dissolved frequency to the next pulse at the dissolved frequency. Thus, the effective TR for this sequence is 8 ms. Using the concept of flip-angle/TR equivalence,[18] the flip angle is then set such that $TR_{90,equiv}$ = 249 ms, the value associated with the parameters recommended by the ^{129}Xe MRI Clinical Trials Consortium.[2] Similar to the dedicated gas exchange sequence, dummy pulses were applied to deplete downstream magnetization, but in this case a stronger flip angle was available (50°), and thus only 10 dummy pulses were used. A sequence timing diagram for this single-breath method is shown in Figure 1. This strategy allows the simultaneous acquisition of ventilation images with nominal resolution of

$4.2 \times 4.2 \times 4.2\ mm^3$ and gas exchange images with nominal resolution of $6.25 \times 6.25 \times 6.25\ mm^3$, competitive with current standards.[2] The total scan duration is ~10 s.

Herein, ventilation and gas exchange image sets acquired within the same breath using the proposed sequence are referred to as “single-breath ventilation” and “single-breath gas exchange,” respectively. Parameters for single-breath ventilation/gas exchange imaging are shown in Table 1. Note that the dissolved bandwidth is slightly reduced in the single-breath method in order to increase signal intensity. T_2^* of ^{129}Xe in membrane and RBCs is ~0.75 to 1 ms, which affords a slightly longer readout duration than is typically used. Given the low SNR inherent in this method, the marginal gains from a slightly reduced bandwidth were considered to be important.

^1H Anatomic Image

^1H anatomic images were also acquired within each breath-hold, immediately after xenon imaging. These images were acquired using the same 3D spiral imaging sequence used for ventilation imaging. Images were acquired such that their geometry (voxel dimensions) matched the respective xenon images. Readout duration, number of spirals, and undersampling parameters were tailored such that the total duration for this sequence was <3.5s (shown in Table 2).

Image Analysis Pipeline

Images were analyzed using a homebuilt, fully automated reconstruction pipeline developed in MATLAB (github.com/pniedbalski3/All_in_one_Xenon_Analysis). Briefly, images are reconstructed using open-source reconstruction tools developed in MATLAB,[26,27] the code for which has been integrated into the above shared github package. For single-breath ventilation/gas exchange images, a schematic of analysis is shown in figure 2. Two images of gaseous xenon were reconstructed, one at the acquired matrix size of 96 x 96 x 96, and one subsampled by truncating the spiral k-space data to correspond to a matrix size of 64 x 64 x 64 (i.e. using only k-space data out to a radius of 2/3 the full k-space radius). This was similarly done for ^1H anatomic images. Subsequently, the ^1H image set acquired within the same breath-hold as xenon imaging is segmented using a trained convolutional neural network (CNN). This trained CNN model is available from the corresponding author upon reasonable request. Following segmentation, gas exchange images are analyzed as described by Wang et al.[17] Note that the first 20 dissolved projections were discarded prior to image reconstruction to ensure that the dissolved magnetization was in a “steady state”, which we identify as the point at which the dissolved signal intensity decays at the same rate as the gaseous signal intensity (i.e. signal loss is primarily due to T_1 relaxation rather than RF or exchange). Moreover, dedicated gas exchange images were reconstructed using only 1218 out of 1900 projections (discarding the first 20 and the last 662 projections) in order to match the number of projections in the single breath acquisition and thus better compare the two.

There are a variety of published methods for analyzing ventilation images to calculate ventilation defect percentage (VDP).[28] As such, our pipeline automatically calculates VDP using several of the most common methods, including mean anchored linear binning,[29,30] linear binning based on a reference population,[31] and Atropos.[32] For the current work, we used the VDP calculated via mean anchored linear binning to compare dedicated and single breath imaging methods.

To compare the single breath protocol to the dedicated protocols, we compared normalized SNR (SNR_n) from ventilation and total dissolved signal images using paired t-tests. This is defined as:

$$SNR_n = \frac{SNR}{DEV \times V_{vox}}, \text{ with } SNR = \frac{mean(signal)}{stdev(noise)}$$

The mean of the signal was found by taking the overall mean of the xenon image within the thoracic cavity mask. A noise mask was generated by dilating the thoracic cavity mask by 7 voxels using a spherical structuring element in order to avoid partial volume effects and image artifacts. Voxels outside of this dilated mask were used to calculate the standard deviation of the noise. For ease of interpretation, all SNR_n values are reported in units of 10^{-3} mL^{-2}.

Line analysis was used to compare the true spatial resolution achieved by imaging methods. Image similarity for ventilation images and dissolved images acquired using the two methods were compared using structural similarity (SSIM) and peak SNR (PSNR). Whole-lung imaging biomarkers, including ventilation defect percent, mean RBC/Gas, and mean membrane/gas, as well as %high membrane, %low membrane, and %low RBC relative to a reference population, were compared using intraclass correlation. %high RBC was not compared as there were only a negligible number of voxels within this bin for the individuals imaged herein. Finally, regions of normal signal (i.e., ventilated regions and membrane or RBC regions within 1 standard deviation of the healthy reference mean) were compared on a regional basis using Dice coefficients and the average distance metric.[33] For these metrics, a Dice coefficient of 1 indicates perfect overlap, while an average distance metric of 0 indicates perfect overlap.

RESULTS

The mean DEV delivered for dedicated ventilation imaging was 119 ± 68 mL (^{129}Xe polarization: 22% ± 7% at time of imaging). For dedicated gas exchange imaging, the mean DEV was 187 ± 23 mL (^{129}Xe polarization: 29% ± 4%). Finally, the mean DEV for single-breath imaging was 231 ± 39 mL (^{129}Xe polarization: 35% ± 4%). These differences are driven by the lower volume of xenon in ventilation doses and by the ordering of scans (single-breath always last) which allows for greater relaxation of hyperpolarized signal in the doses that have a longer time between dispensing and delivery. Specifically, doses require 20-30 minutes to prepare, so doses for the first scans were stored in a static magnetic field for up to 45 min prior to delivery to subjects. T_1 ~ 1hr in this “storage” magnetic field, so up to 50% of initial polarization was lost for dedicated ventilation and gas exchange scans.

Images were successfully acquired and reconstructed for all subjects. The single breath acquisition for ventilation and gas exchange required approximately the same duration as each of the dedicated scans. There were no significant image artifacts in any of the acquired images. SNR was adequate for analysis (>10) for all subjects and scan types. The mean SNR for dedicated ventilation images was 22.5 (Range 14.0 to 32.6) and the mean SNR for dedicated total dissolved images was 25.7 (Range 17.6 to 40.9). Single-Breath ventilation images had mean SNR 34.3 (Range 22.6 to 47.3) and single-breath total dissolved images had mean SNR 45.0 (Range 32.1 to 61.7). Representative images are shown in figure 3.

To effectively compare SNR between imaging types, we must account for the different DEVs and voxel volumes of each image acquisition, for which we use the normalized SNR (in units of $10^{-3}mL^{-2}$) described above. For dedicated ventilation, SNR_n was 3.4 (Range 1.7 to 5.0), while for single-breath ventilation, SNR_n was 2.1 (Range 1.0 to 3.0), $p = 0.007$. Dedicated total dissolved images had SNR_n of 0.57 (Range 0.37 to 0.91) and single-breath total dissolved images had SNR_n of 0.83 (Range 0.53 to 1.3), $p = 0.17$.

Ventilation images acquired via a dedicated breath-hold and via the single-breath protocol had high qualitative agreement. Images appeared visually similar and similar quantity, shape, and size of ventilation defects were present in both images. Mean SSIM for ventilation images was 0.52 (Range 0.38 to 0.62), and mean PSNR was 22.3 (Range 20.2 to 24.3). Ventilation images acquired via the single breath protocol had, to the naked eye, slightly poorer resolution than images acquired in a dedicated breath-hold, which is consistent with the lower nominal resolution at which they were acquired. Line analysis (comparison of signal profiles along corresponding lines in the images) showed that the additional blurring in the single breath method was less than 1 pixel, with only slightly reduced edge fidelity (Figure 4).

Whole-lung and regional comparisons are summarized in Table 3. Ventilation defect percent ranged from 4.7 to 22.2% for images acquired during a dedicated breath-hold and from 1.6 to 17.3% for single breath images. Bland Altman analysis showed a systematic difference of about 2 percentage points between the two methods, with single-breath ventilation images typically showing lower VDP (Figure 5). However, the intraclass correlation between measures of VDP was strong, (ICC = 0.77, $p = 0.01$).

Gas exchange images acquired using both methods showed reasonable qualitative agreement. SSIM for total dissolved images was 0.71 (Range 0.65 to 0.79) and PSNR was 26.3 (Range 25.8 to 27.3). Following separation of membrane and RBC images, the SSIM and PSNR for membrane/gas images were 0.48 (Range 0.44 to 0.56) and 25.3 (Range 24.7 to 26.3), respectively. For RBC, SSIM and PSNR were 0.14 (Range 0.07 to 0.23) and 20.3 (Range(17.7 to 22.5). Defects, low regions, normal regions, and high regions on binned images appeared in similar locations and had similar extent in both types of images (Figure 6). While there were small regions of low or high signal that appeared in only one image, all large defects (> 20 voxels) were clearly visible in both images.

The mean Membrane/Gas and RBC/Gas ratios were comparable for both imaging methods, with better agreement for the Membrane/Gas ratio. Bland Altman analysis showed a systematic difference of about 3.4% for the Membrane/Gas ratio, and a difference of 4.8% for the RBC/Gas ratio. Once again, the intraclass correlation between the two imaging methods was strong, with ICC = 0.97, $p = 0.001$ for membrane/gas and ICC = 0.99, $p < 0.001$ for RBC/gas.

Regional image comparison methods, including Dice coefficients and the average distance metric showed reasonable agreement for all methods. When comparing ventilated regions of the lungs, the mean Dice coefficient was 0.92 (range: 0.88 to 0.94). Similarly, when comparing Membrane/Gas and RBC/Gas in the “normal” range, mean dice coefficients were 0.82 (range: 0.73 to 0.90) and 0.73 (range: 0.58 to 0.80), respectively. Mean Average Distance for ventilated regions, normal membrane, and normal RBC were 0.08 (range: 0.05 to 0.13), 0.19 (range: 0.10 to 0.29), and 0.33 (range: 0.24 to 0.55), respectively. The mean Dice coefficient for ventilation defect regions was 0.27 (range: 0.02 to 0.69), and the mean average distance was 4.94 (range: 0.52 to 14.01). Similarly, the mean Dice coefficient for low membrane regions was 0.40 (range: 0.09 to 0.59) and the mean average distance was 1.5 (range: 0.6 to 4.49). The mean Dice coefficient for low RBC regions was 0.60 (range: 0.54 to 0.69) and the mean average distance was 0.50 (range: 0.39 to 0.60).

In our one participant imaged twice using the single-breath acquisition, we observed similar results as when comparing dedicated and single-breath acquisitions. Ventilation images had strong visual similarity and nearly identical VDP calculation. Membrane and RBC images showed similar large features with some discrepancies in smaller features (Figure 7).

DISCUSSION

In comparison to previously published methods for ventilation and gas exchange imaging, the proposed single breath ventilation/gas exchange imaging sequence is capable of producing comparable images within a single breath-hold of similar or even shorter duration than the breath-holds required for dedicated imaging.[2] Furthermore, the comparatively short breath-hold used for single-breath imaging (~10 s) provides sufficient time for an anatomic image set to be acquired within the same breath-hold for a total breath-hold duration of ~14 s. As has been previously described,[6] this greatly simplifies and improves image analysis by mitigating the need for image registration between two separate breath-holds.

For this single-breath method, it was expected that gas exchange imaging would produce comparable results to the dedicated imaging method. Specifically, gas exchange images are acquired using a 3D radial 1-point Dixon strategy that is identical to previously published methods,[12] save for differences in TR and flip angle. As we have shown previously, flip-angle/TR equivalence[18] allows us to tailor the TR and flip angle for optimal use of the imaging time without impacting the qualitative or quantitative character of images.[19]

However, it was unclear how the acquisition of a higher resolution ventilation image during gas exchange imaging would impact measurements. In particular, the use of a larger flip angle and different sampling scheme for gas acquisition (as compared to standard gas exchange imaging) may lead to different quantitative values or qualitative appearance during analysis. Different sampling schemes could lead to different undersampling artifacts in the gas images than in the dissolved images. An example of this is visible in the representative images shown in figure 2. Because the low-resolution gas image is generated by reconstructing only the central portion of a spiral k-space acquisition, the gaseous image is nearly fully sampled, while the dissolved image is only ~16% fully sampled. Thus, the dissolved image has greater blurring and several of the ventilation defects that are observed in the low-resolution gas image (Figure 2A) appear to have normal dissolved signal (Figure 2B). This could potentially lead to artificially elevated membrane or RBC signal due as a result of scaling by the gas signal (i.e. sharper defects in the gas image would have lower signal intensity than a more undersampled/blurred gas image, leading to larger membrane/gas or RBC/gas values). However, this appeared to have only a minimal impact in our data, as there was only a small systematic difference between dedicated and single-breath membrane and RBC values (Figure 5), with single-breath yielding lower values in both cases.

Membrane/gas showed a systematic difference of 0.028 (3.5%), and RBC/gas showed a difference of 0.012 (4.8%) between the two methods. Reports on the repeatability of gas exchange Xe-MRI are limited, but our measured difference falls well within the ranges that have been reported for repeatability.[34] Of note, this study is different from our own in two respects. First, rather than collecting images in two breath-holds back-to-back, it collected images 1 month apart. Second, it showed differences between the two measurements scattered on both sides of 0, whereas our single-breath measurements are consistently smaller than our dedicated measurements. The smaller values measured with the single breath method could simply be explained by our small sample size. The fact that the single-breath acquisition always took place after the dedicated scan may also play a role. This may be due to physical (i.e. dedicated scans happening first leads to lower SNR which could inflate measurements) or physiological (e.g. pulmonary vasoconstriction from previous xenon breath-holds and prolonged supine position in the scanner) reasons. We note that the mean SNR for dissolved images was very much lower for dedicated gas exchange scanning (25 ± 9) was very much lower than single-breath (45 ± 11). This lower SNR, despite being adequate for analysis, could contribute to differences between the methods. Finally, it could be that differences in lung volume between the two scans led to differences between scan types. The total lung inflation for the two gas exchange scans was roughly equivalent (within 4%) for 4 out of 5 scans. For the 5th, the lung inflation was 17% greater for the single breath scan. The difference between scan types was 0.05 for mean membrane/gas and 0.02 for mean RBC/gas. Thus, while lung inflation may have an impact on Xe-MRI markers, differences in lung inflation do not appear to have a strong effect on our comparison of dedicated and single breath methods.

While regional agreement was generally moderate to good (based on qualitative examination, SSIM, PSNR, dice coefficients, and average distance), there were several features that suggested poorer agreement. In particular, SSIM for RBC images was very low. This is likely due to the low resolution and low SNR that is a common feature of RBC images. Despite very low SSIM, other measures including PSNR, average distance, and dice coefficients suggest better quantitative regional agreement. In addition, large features were discernable in both images, but there were smaller regions of defect or high signal that were only visible in one of the two. Most likely, this reflects the relatively poor spatial resolution achieved by this imaging method. While images are reconstructed to a nominal resolution of 6.25 x 6.25 x 6.25 mm^3, the true resolution is significantly poorer than this. Thus, small defects are expected to be less repeatable than larger defects.

Ventilation images showed greater discrepancies between the two methods. To begin with, dedicated ventilation imaging had significantly higher SNR_n than single-breath imaging. This is due to the larger flip angle used for acquisition of dedicated ventilation imaging. However, this reduction in SNR_n is of minimal concern for the single-breath method due to the larger xenon DEV typically delivered for gas exchange imaging as compared to ventilation imaging.[2] This larger DEV leads to similar or greater SNR for the single-breath method despite lower SNR_n. Single-breath imaging consistently produced lower VDP than dedicated imaging, though the measurements had good intraclass correlation. Moreover, Dice coefficient and average distance metrics showed relatively poor regional agreement for the location of defects. This is in part due to the relatively minimal ventilation impairment observed in our subject population. Only 5 of 11 subjects showed significant ventilation impairment (VDP > 10%), with the rest having little to no impairment (VDP < 5%). As such, the small number of voxels considered as defects is likely driving the low Dice coefficient and high average distance. Furthermore, it is known that there is some variation in the location and extent of ventilation defects across multiple breath-holds, which could also contribute to this poor regional agreement.[35] Examining agreement between ventilated regions provided high Dice coefficients and low average distance, signaling good regional agreement in these larger regions of interest.

Part of the discrepancy between VDP measurements may be the higher resolution of the dedicated ventilation image (4 x 4 x 4 mm^3 voxel size) as compared to the single-breath ventilation image (4.2 x 4.2 x 4.2 mm^3 voxel size). This slight difference in resolution is apparent from line analysis and even to the unassisted eye in some images. Such a difference could lead to partial volume effects in defects, which may cause some defects to be classified as normal in the lower resolution image. Increased sophistication in analysis[36] or reconstructing images to higher resolution may alleviate these differences.

It is also possible that the acquisition of dissolved phase signal in between subsequent acquisitions of the gas-phase signal may impact ventilation images by the exchange between gaseous and dissolved compartments. Notably, it is on this principle that xenon polarization transfer contrast (XTC) operates, though in XTC the dissolved signal is fully saturated between acquisitions of gas signal.[37,38] In this case, we use a comparatively small flip angle and achieve a steady state dissolved signal. Because the signal is at a steady state, it is unlikely that the exchange between gaseous and dissolved reservoirs leads to relevant changes to the ventilation signal as compared to the dedicated scan in which dissolved signal is not directly excited.

Though not the primary focus of our manuscript, we note that the post-COVID-19 participants imaged for this study show similar Xe-MRI markers to what has been observed previously.[39-42] Namely, we observed minimal ventilation defects and a reduced RBC/membrane signal as compared to healthy reference values.

While this method shows promise for simplifying and shortening Xe-MRI sessions, the present study has several limitations. Our sample size is relatively small, using only enough subjects to show the proof of concept. Related to this, we imaged no patients with significant imaging abnormalities; only one patient had significant ventilation defects. While RBC defects were common in our small sample size, there were very few high membrane regions as would be expected in other patient populations such as interstitial lung disease. Finally, our imaging method still requires a calibration scan in order to calibrate scanner frequency, transmit pulse amplitude, and RBC/membrane ratio, as was performed in this study. For future work, we intend to incorporate calibration routines into this single-breath imaging sequence so as to have a one-breath-hold protocol for hyperpolarized ^{129}Xe MRI.

The data that support the findings of this study are available on request from the corresponding author. The data are not publicly available due to privacy or ethical restrictions.

CONCLUSIONS

We have developed and applied a single breath MRI protocol for collecting hyperpolarized ^{129}Xe ventilation and gas exchange images plus an anatomic image for thoracic cavity masking all within a single ~14 s breath-hold (~10 s for Xe-MRI, ~3.5 s for ^{1}H). This method produces images that are competitive with current standards in terms of resolution and SNR. Moreover, the qualitative appearance and quantitative analysis of images appears to be minimally affected by the accelerated method. This image sequence was developed using a combination of standard Xe-MRI radial 1-point Dixon imaging and “FLORET,” a 3D spiral approach with open-source gradient calculations available. Most importantly, this method enables the acquisition of the two most potentially-clinically relevant Xe-MRI contrasts (ventilation and gas exchange) in one breath-hold rather than two, reducing the cost of this technique by 50% and reducing the number of breath-holds required of patients. As Xe-MRI increases in research use and approaches clinical adoption, this single-breath protocol may accelerate adoption of the Xe-MRI technique.

ACKNOWLEDGEMENTS

This work was supported by the American Heart Association (Career Development Award 930177) and the Scleroderma Foundation (New Investigator Award). All imaging was performed at the Hoglund Biomedical Imaging Center, which is supported by Forrest and Sally Hoglund and the NIH: S10 RR29577

Grant Support:

This work was supported by the KUMC Research Institute, The Scleroderma Foundation (New Investigator Award), the American Heart Association (Career Development Award 930177), and Polarean Imaging, Plc.

Abbreviations:

Xe-MRI	Hyperpolarized ^{129}Xe MRI
RBC	Red Blood Cell
TE_{90}	Echo time at which Membrane and RBC signals are 90° out of phase

References:

1. Mugler JP, Altes TA. Hyperpolarized 129Xe MRI of the human lung. J Magn Reson Imaging. 2013;37:313–331. [PubMed: 23355432]
2. Niedbalski PJ, Hall CS, Castro M, et al. Protocols for multi-site trials using hyperpolarized 129Xe MRI for imaging of ventilation, alveolar-airspace size, and gas exchange: A position paper from the 129Xe MRI clinical trials consortium. Magn Reson Med. 2021;86:2966–2986. [PubMed: 34478584]
3. Doganay O, Matin TN, Mcintyre A, et al. Fast dynamic ventilation MRI of hyperpolarized 129Xe using spiral imaging. Magn Reson Med. 2018;79:2597–2606. [PubMed: 28921655]
4. Zanette B, Friedlander Y, Munidasa S, Santyr GE. Comparison of 3D stack-of-spirals and 2D gradient echo for ventilation mapping using hyperpolarized 129Xe. Proc Intl Soc Mag Reson Med. 2020;28:0449.
5. Zanette B, Santyr G. Accelerated interleaved spiral-ideal imaging of hyperpolarized 129Xe for parametric gas exchange mapping in humans. Magn Reson Med. 2019;82:1113–1119. [PubMed: 30989730]
6. Collier GJ, Hughes PJC, Horn FC, et al. Single breath-held acquisition of coregistered 3D 129Xe lung ventilation and anatomical proton images of the human lung with compressed sensing. Magn Reson Med. 2019;82:342–347. [PubMed: 30821003]
7. Willmering MM, Niedbalski PJ, Wang H, et al. Improved pulmonary 129Xe ventilation imaging via 3D-spiral UTE MRI. Magn Reson Med. 2020;84:312–320. [PubMed: 31788858]
8. Zhou Q, Li H, Rao Q, et al. Assessment of pulmonary morphometry using hyperpolarized 129Xe diffusion-weighted MRI with variable-sampling-ratio compressed sensing patterns. Med Phys. 2023;50:867–878. [PubMed: 36196039]
9. Duan C, Deng H, Xiao S, et al. Accelerate gas diffusion-weighted MRI for lung morphometry with deep learning. Eur Radiol. 2022;32:702–713. [PubMed: 34255160]
10. Zanette B, Munidasa S, Friedlander Y, Ratjen F, Santyr G. A 3D stack-of-spirals approach for rapid hyperpolarized 129Xe ventilation mapping in pediatric cystic fibrosis lung disease. Magn Reson Med. 2023;89:1083–1091. [PubMed: 36433705]
11. Kaushik SS, Cleveland ZI, Cofer GP, et al. Diffusion weighted imaging of hyperpolarized 129Xe in patients with chronic obstructive pulmonary disease. Magn Reson Med. 2011;65:1154–1165. [PubMed: 21413080]
12. Kaushik SS, Robertson SH, Freeman MS, et al. Single-breath clinical imaging of hyperpolarized Xe-129 in the airspaces, barrier, and red blood cells using an interleaved 3D radial 1-point dixon acquisition. Magn Reson Med. 2016;75:1434–1443. [PubMed: 25980630]
13. Kirby M, Ouriadov A, Svenningsen S, et al. Hyperpolarized 3He and 129Xe magnetic resonance imaging apparent diffusion coefficients: Physiological relevance in older never- and ex-smokers. Physiol Rep. 2014;2:e12068. [PubMed: 25347853]
14. Collier GJ, Eaden JA, Hughes PJC, et al. Dissolved 129Xe lung MRI with four-echo 3D radial spectroscopic imaging: Quantification of regional gas transfer in idiopathic pulmonary fibrosis. Magn Reson Med. 2021;85:2622–2633. [PubMed: 33252157]
15. Hahn AD, Kammerman J, Fain SB. Removal of hyperpolarized 129Xe gas-phase contamination in spectroscopic imaging of the lungs. Magn Reson Med. 2018;80:2586–2597. [PubMed: 29893992]
16. Wang Z, Rankine L, Bier EA, et al. Using hyperpolarized 129Xe gas-exchange MRI to model the regional airspace, membrane, and capillary contributions to diffusing capacity. J Appl Physiol. 2021;130:1398–1409. [PubMed: 33734831]
17. Wang Z, Robertson SH, Wang J, et al. Quantitative analysis of hyperpolarized 129Xe gas transfer MRI. Med Phys. 2017;44:2415–2428. [PubMed: 28382694]
18. Ruppert K, Amzajerdian F, Hamedani H, et al. Assessment of flip angle–tr equivalence for standardized dissolved-phase imaging of the lung with hyperpolarized 129Xe MRI. Magn Reson Med. 2019;81:1784–1794. [PubMed: 30346083]
19. Niedbalski PJ, Lu J, Hall CS, et al. Utilizing flip angle/tr equivalence to reduce breath hold duration in hyperpolarized 129Xe 1-point dixon gas exchange imaging. Magn Reson Med. 2022;87:1490–1499. [PubMed: 34644815]

20. He M, Robertson SH, Kaushik SS, et al. Dose and pulse sequence considerations for hyperpolarized 129Xe ventilation MRI. Magn Reson Imaging. 2015;33:877–885. [PubMed: 25936684]
21. Pipe JG, Zwart NR, Aboussouan EA, Robison RK, Devaraj A, Johnson KO. A new design and rationale for 3D orthogonally oversampled k-space trajectories. Magn Reson Med. 2011;66:1303–1311. [PubMed: 21469190]
22. Robison RK, Anderson AG, Pipe JG. Three-dimensional ultrashort echo-time imaging using a floret trajectory. Magn Reson Med. 2017;78:1038–1049. [PubMed: 27775843]
23. Pipe JG, Menon P. Sampling density compensation in MRI: Rationale and an iterative numerical solution. Magn Reson Med. 1999;41:179–186. [PubMed: 10025627]
24. Pipe JG, Zwart NR. Spiral trajectory design: A flexible numerical algorithm and base analytical equations. Magn Reson Med. 2014;71:278–285. [PubMed: 23440770]
25. Qing K, Ruppert K, Jiang Y, et al. Regional mapping of gas uptake by blood and tissue in the human lung using hyperpolarized xenon-129 MRI. J Magn Reson Imaging. 2014;39:346–359. [PubMed: 23681559]
26. Robertson SH, Virgincar RS, Bier EA, et al. Uncovering a third dissolved-phase 129Xe resonance in the human lung: Quantifying spectroscopic features in healthy subjects and patients with idiopathic pulmonary fibrosis. Magn Reson Med. 2017;78:1306–1315. [PubMed: 28940334]
27. Robertson SH, Virgincar RS, He M, Freeman MS, Kaushik SS, Driehuys B. Optimizing 3D noncartesian gridding reconstruction for hyperpolarized 129Xe MRI—focus on preclinical applications. Concept Magn Reson A. 2015;44:190–202.
28. Roach DJ, Willmering MM, Plummer JW, et al. Hyperpolarized (129)xenon MRI ventilation defect quantification via thresholding and linear binning in multiple pulmonary diseases. Acad Radiol. 2022;29 Suppl 2:S145–s155.
29. Thomen RP, Walkup LL, Roach DJ, Cleveland ZI, Clancy JP, Woods JC. Hyperpolarized 129Xe for investigation of mild cystic fibrosis lung disease in pediatric patients. J Cyst Fibros. 2017;16:275–282. [PubMed: 27477942]
30. Thomen RP, Sheshadri A, Quirk JD, et al. Regional ventilation changes in severe asthma after bronchial thermoplasty with 3He MR imaging and ct. Radiology. 2015;274:250–259. [PubMed: 25144646]
31. He M, Driehuys B, Que LG, Huang YCT. Using hyperpolarized Xe-129 MRI to quantify the pulmonary ventilation distribution. Acad Radiol. 2016;23:1521–1531. [PubMed: 27617823]
32. Tustison NJ, Avants BB, Flors L, et al. Ventilation-based segmentation of the lungs using hyperpolarized He-3 MRI. J Magn Reson Imaging. 2011;34:831–841. [PubMed: 21837781]
33. Taha AA, Hanbury A. Metrics for evaluating 3D medical image segmentation: Analysis, selection, and tool. BMC Med Imaging. 2015;15:29–29. [PubMed: 26263899]
34. Hahn AD, Kammerman J, Evans M, et al. Repeatability of regional pulmonary functional metrics of hyperpolarized 129Xe dissolved-phase MRI. J Magn Reson Imaging. 2019;50:1182–1190. [PubMed: 30968993]
35. Woodhouse N, Wild JM, van Beek EJR, Hoggard N, Barker N, Taylor CJ. Assessment of hyperpolarized 3He lung MRI for regional evaluation of interventional therapy: A pilot study in pediatric cystic fibrosis. J Magn Reson Imaging. 2009;30:981–988. [PubMed: 19856418]
36. Tustison NJ, Altes TA, Qing K, et al. Image- versus histogram-based considerations in semantic segmentation of pulmonary hyperpolarized gas images. Magn Reson Med. 2021;86:2822–2836. [PubMed: 34227163]
37. Ruppert K, Brookeman JR, Hagspiel KD, Mugler JP. Probing lung physiology with xenon polarization transfer contrast (xtc). Magn Reson Med. 2000;44:349–357. [PubMed: 10975884]
38. Ruppert K, Mata JF, Wang HTJ, et al. Xtc MRI: Sensitivity improvement through parameter optimization. Magn Reson Med. 2007;57:1099–1109. [PubMed: 17534927]
39. Li H, Zhao X, Wang Y, et al. Damaged lung gas exchange function of discharged covid-19 patients detected by hyperpolarized ^{129}Xe MRI. Science Advances. 2021;7:eabc8180. [PubMed: 33219111]

40. Grist JT, Chen M, Collier GJ, et al. Hyperpolarized 129Xe MRI abnormalities in dyspneic participants 3 months after covid-19 pneumonia: Preliminary results. Radiology. 2021;301:E353–E360. [PubMed: 34032513]
41. Grist JT, Collier GJ, Walters H, et al. Lung abnormalities depicted with hyperpolarized xenon MRI in patients with long covid. Radiology. 2022;0:220069.
42. Matheson AM, McIntosh MJ, Kooner HK, et al. Persistent 129Xe MRI pulmonary and ct vascular abnormalities in symptomatic individuals with post-acute covid-19 syndrome. Radiology. 2022;305:466–476. [PubMed: 35762891]

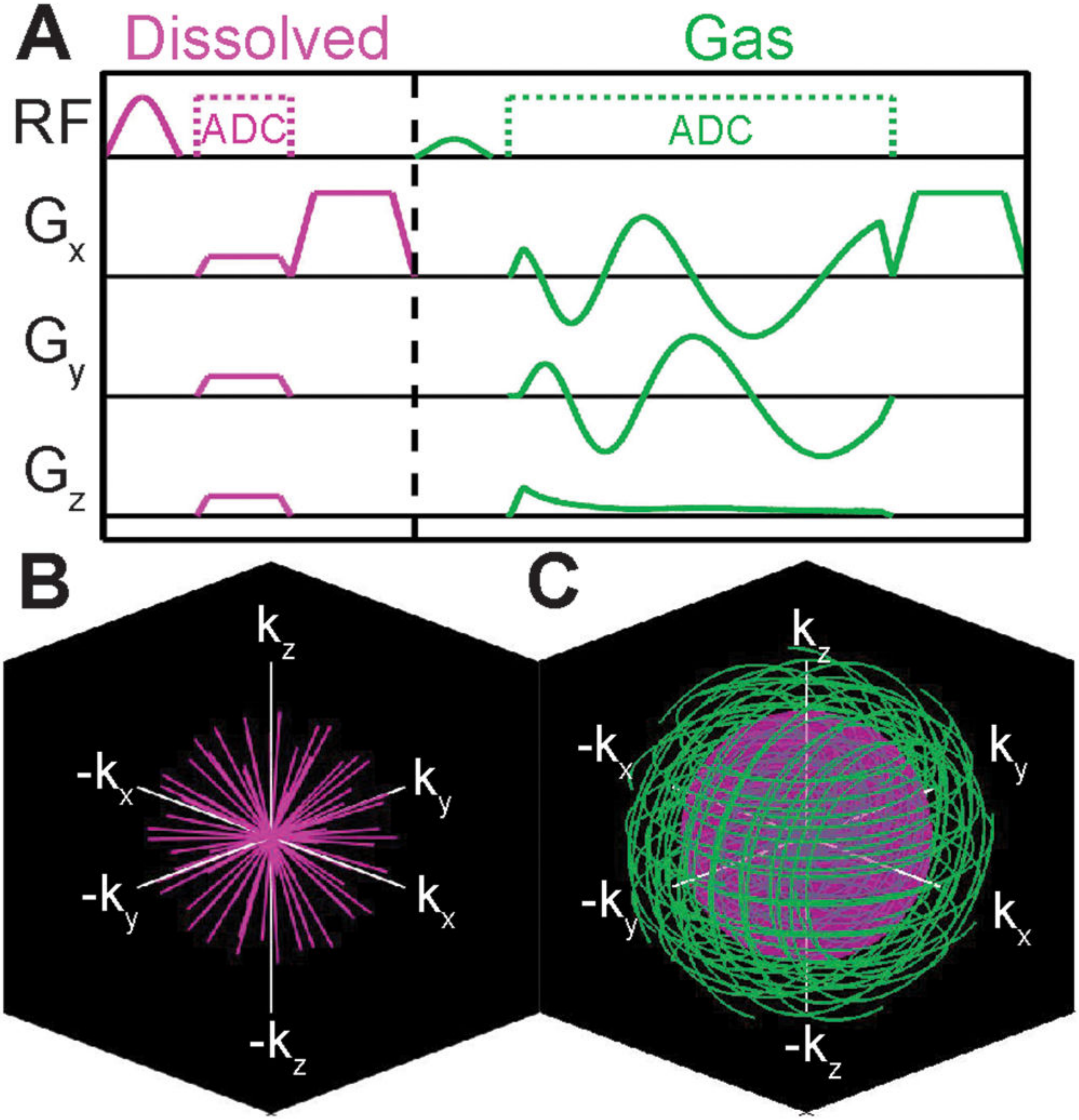

Figure 1.

A Sequence timing diagram for the proposed single-breath ventilation/gas exchange sequence. Dissolved ^{129}Xe is sampled using a 3D radial scheme, which is interleaved with 3D Spiral encoding of the gas signal. K-space coverage for the **B** dissolved and **C** gas sampling are shown. The inset sphere in **C** shows the k-space radius of the dissolved acquisition.

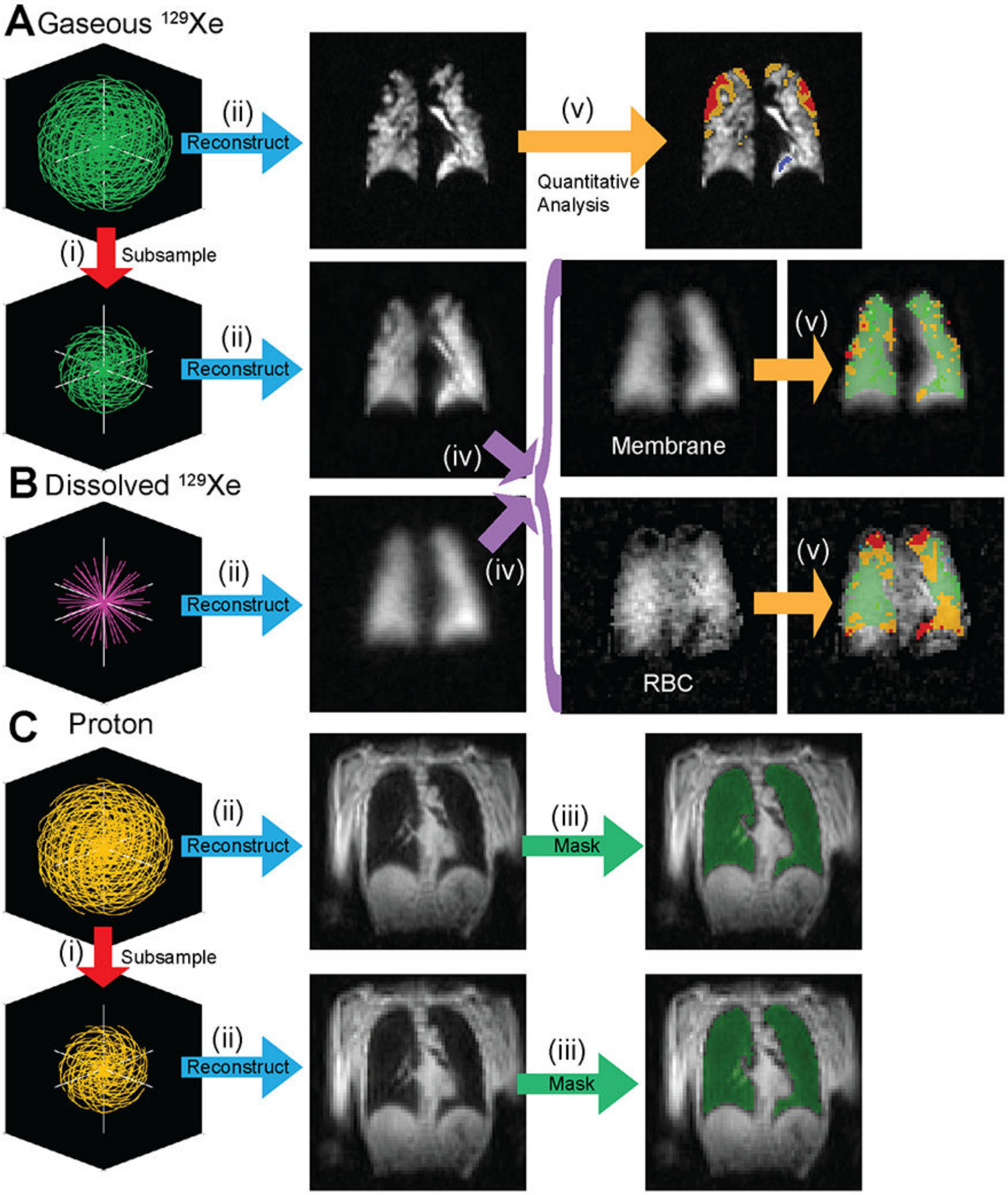

Figure 2.

Overview of the reconstruction and analysis process for the proposed single-breath imaging method. **A** Gas, **B** Dissolved, and **C** ^{1}H raw data are acquired in a single breath-hold. **(i)** Gas and ^{1}H data are subsampled to generate both low-resolution and high-resolution datasets. **(ii)** Data are reconstructed using a narrow reconstruction kernel (Ventilation Image) or a broad reconstruction kernel (dissolved image, low resolution gas). **(iii)** High and low spatial resolution masks are generated from ^{1}H images using a Deep Learning segmentation algorithm. **(iv)** Dissolved and low-resolution gas images are used to separate the membrane and RBC constituents of dissolved images. **(v)** Gas (high resolution), membrane/gas, and RBC/gas images are quantitatively analyzed using previously published methods.

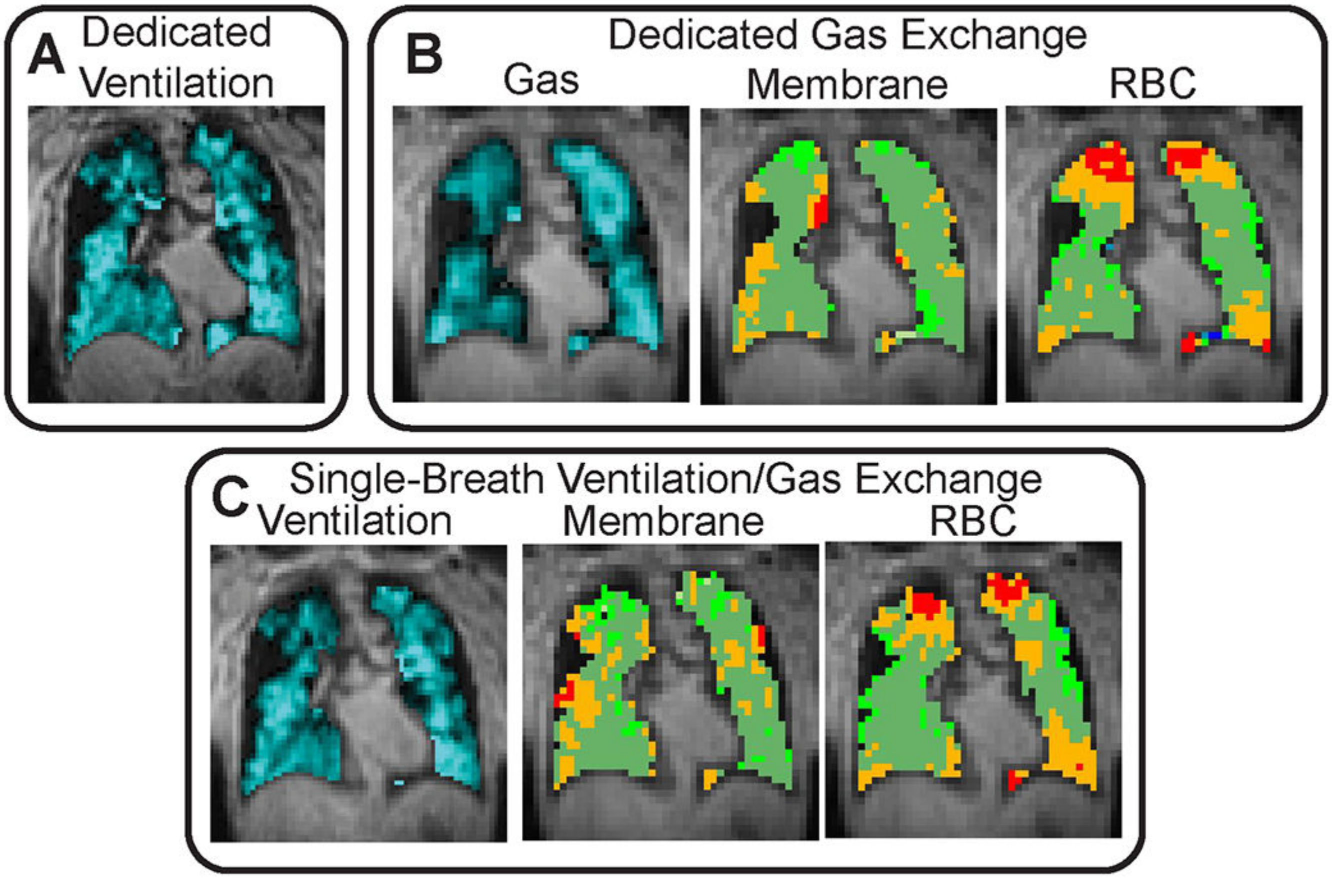

Figure 3.

Representative images for **A** dedicated ventilation scan, **B** dedicated gas exchange scan, and **C** single-breath ventilation/gas exchange scan. There is reasonable qualitative agreement between dedicated and single-breath ventilation scans. More ventilation defects are observed in single-breath gas exchange images (see C Membrane and RBC), likely due to the higher resolution gas-phase image as compared to dedicated gas exchange images. Even so, binned gas exchange images show similar location and extent of "low" and "defect" regions.

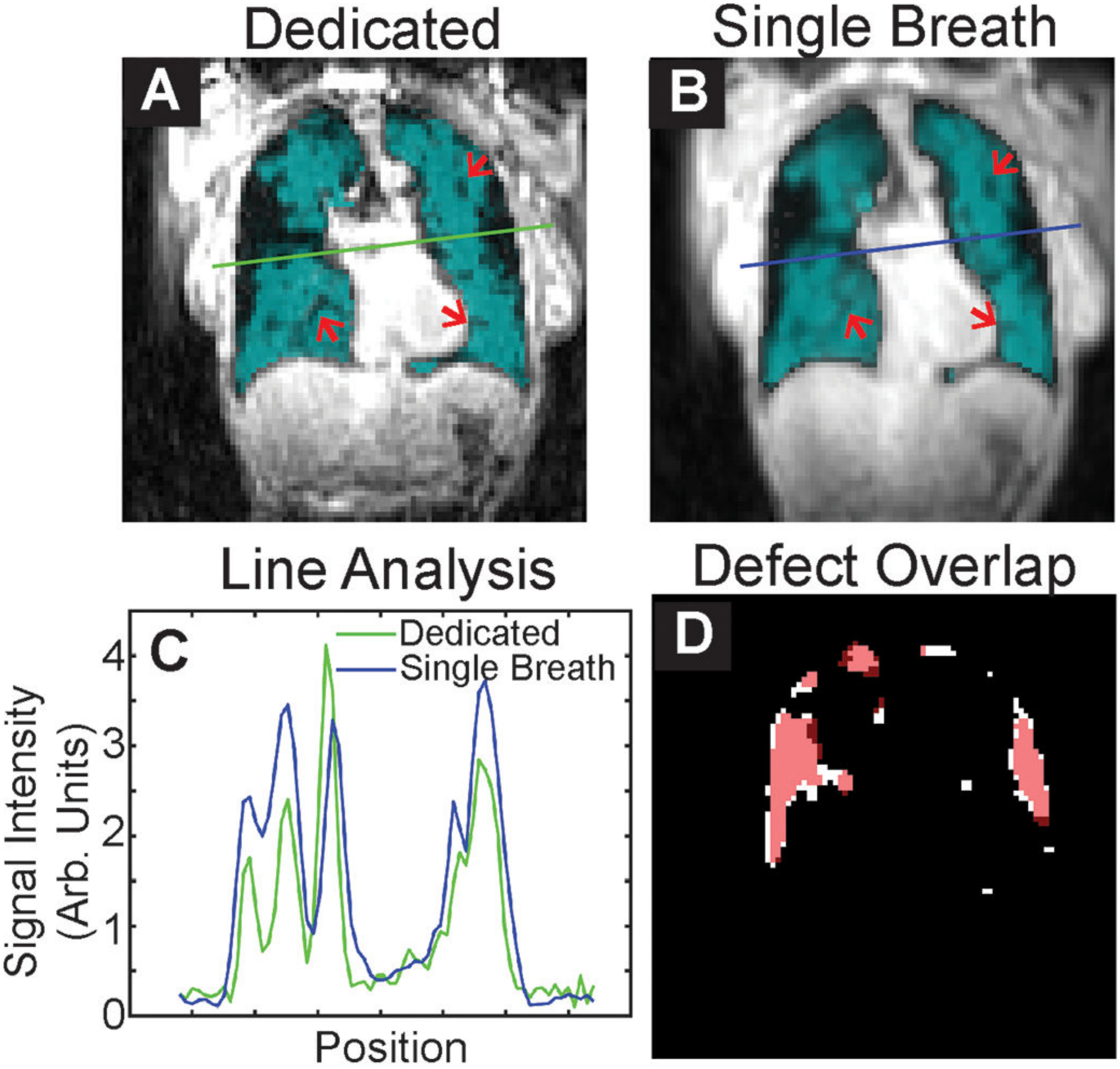

Figure 4.

Representative slices from **A** Dedicated and **B** Single-breath ventilation imaging. Subtle ventilation defects visible in both images are highlighted by arrows. **C** Line analysis shows slightly greater blurring of images for single-breath images, which is expected given the lower resolution of these images (4.2 vs. 4 mm nominal resolution). **D** Overlap of defect maps, with dedicated shown in white and single-breath shown in red. There is considerable overlap of ventilation defects.

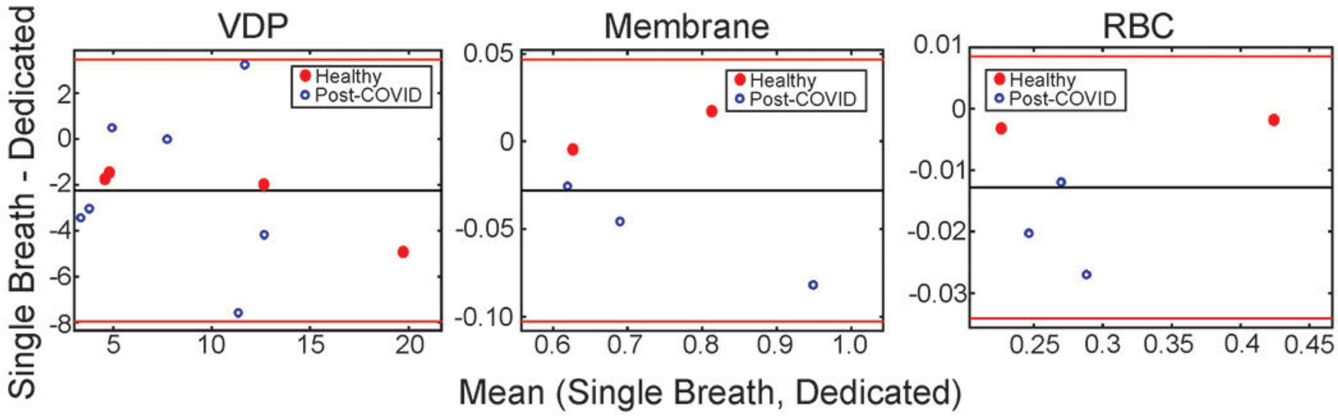

Figure 5.

Bland Altman analysis for ventilation defect percent (VDP), Membrane/gas ratio, and RBC/gas ratio. The single-breath method provides quantitative metrics that appear to be slightly lower than dedicated scanning.

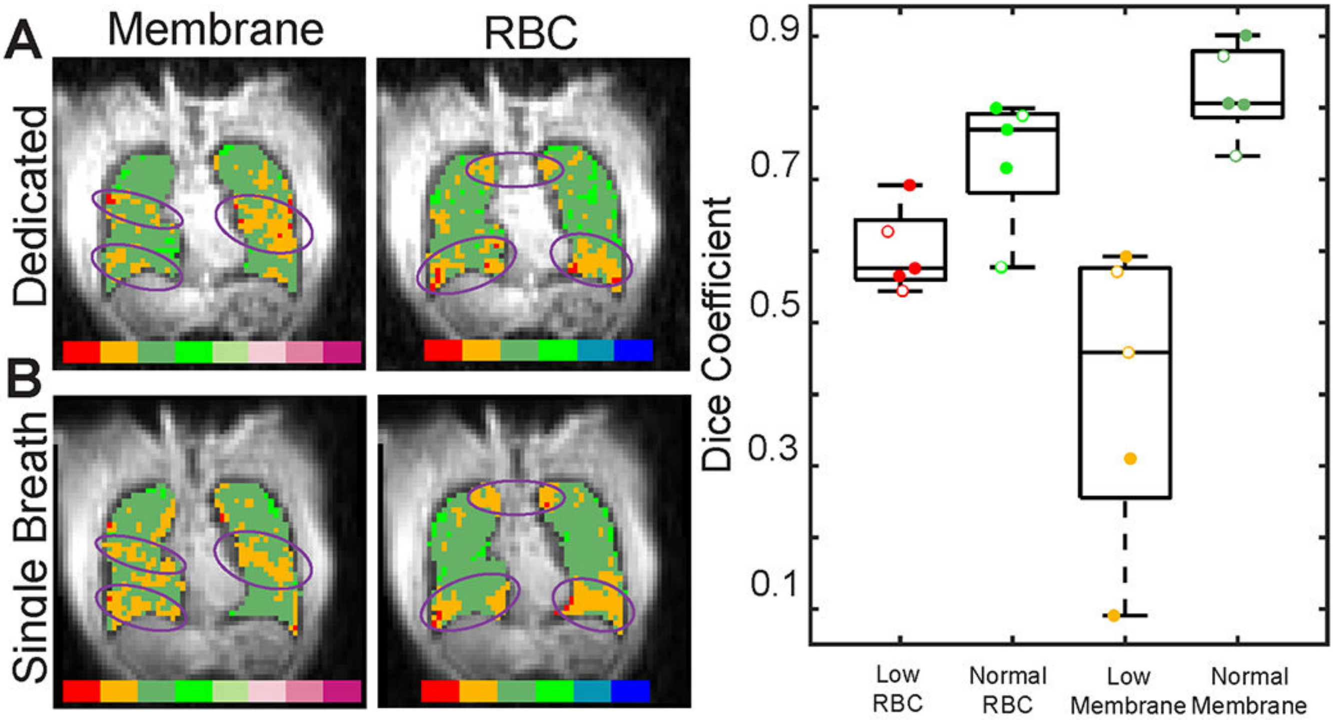

Figure 6.

Representative slices from **A** dedicated and **B** single breath gas exchange imaging for a post-COVID-19 subject. There is reasonable qualitative agreement between the two acquisition methods. Prominent features that are similar in both dedicated and single-breath imaging are highlighted by purple ovals. **C** Dice coefficients show moderate to good regional agreement for regions of normal and low membrane and RBC signal. Healthy participant data is shown with open circles. Note that the low Dice coefficients for the two extreme "Low Membrane" points are driven by a very small number of membrane voxels binned low (1.8% and 11% - In comparison, the mean %low RBC was 35% for all participants).

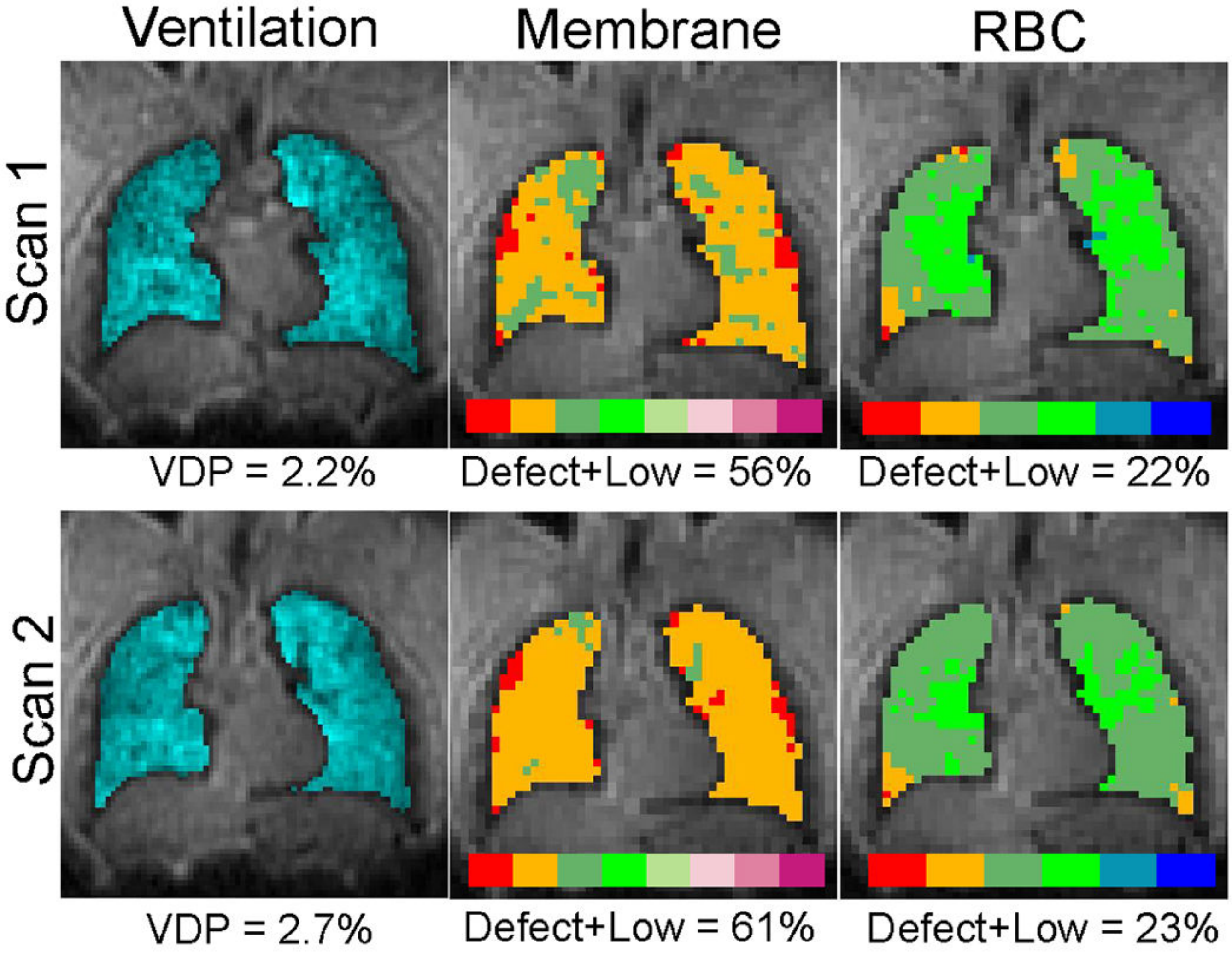

Figure 7.

Representative single-breath acquisition repeated in the same participant about 10 minutes apart. In this preliminary example, there is reasonable agreement between the two scans. Note that the VDP and Defect+Low values reported are whole-lung measurements, whereas we only show a single central slice.

Table 1.

Imaging parameters for the hyperpolarized ^{129}Xe imaging sequences used herein. TE90 refers to the echo time at which Membrane and RBC signals are 90° out of phase at the center of k-space.

Parameter	Dedicated Ventilation	Dedicated Gas Exchange	Single-breath Ventilation/Gas Exchange
Field of View (mm^3)	360x360x360	400x400x400	400x400x400
Gas Matrix Size [1]	90x90x90	64x64x64	96x96x96
Dissolved Matrix Size [1]	---	64x64x64	64x64x64
Gas TR (ms)	7.0	2.7	5.3
Dissolved TR (ms)	---	2.7	2.7
TE (ms)	0.5	TE90 (0.45 – 0.50)	TE90 (0.45 – 0.50)
Gas Flip Angle (°)	2.3	0.5	1
Dissolved Flip Angle (°)	---	12.0	14.6
Gas Bandwidth (Hz/Pixel)	1,044	751	1,635
Dissolved Bandwidth (Hz/Pixel)	---	751	686
Gas Encoding Scheme	FLORET (3D Spiral)	3D Radial	FLORET (3D Spiral)
Dissolved Encoding Scheme	---	3D Radial	3D Radial
Number of projections (Gas) [2]	1062	1900	1238
Number of projections (Dissolved) [2]	---	1900	1238
Xe-MRI Duration (s)	7.4	10.3	9.9
Anatomic MRI Duration (s) [3]	3.8	1.7	3.0
Approximate Total Breath-hold duration (s) [4]	12	13	14

[1] For simplicity, we report the resolution as the nominal resolution (FOV/Cartesian matrix size) throughout. With the non-Cartesian sampling and reconstruction employed here, the true resolution is worse than nominal.

[2] For dedicated gas exchange imaging, 1900 projections were acquired, but 1238 were used for image reconstruction in order to match the undersampling in the single-breath acquisition.

[3] See Table 2 for detailed parameters of ^{1}H anatomic images.

[4] Note that there is ~1s of switching time between Xe-MRI scan and anatomic scan.

Table 2.

Imaging parameters for the anatomic imaging sequences used to generate thoracic cavity masks.

Parameter	Dedicated Ventilation Anatomic	Dedicated Gas Exchange Anatomic	Single-breath Ventilation/Gas Exchange Anatomic
Field of View (mm^3)	360x360x360	400x400x400	400x400x400
Matrix Size	90x90x90	64x64x64	96x96x96
TR/TE (ms)	4.5/0.5	2.8/0.3	3.3/0.3
Flip Angle (°)	5.0	5.0	5.0
Number of Spiral Arms	850	604	906
Bandwidth (Hz/Pixel)	2,899	3,605	2,957
Total Duration (s)	3.8	1.7	3.0

Table 3.

Summary of whole-lung and regional comparisons. Systematic bias refers to the mean difference between single-breath and dedicated measurements. All other values are shown as mean (range).

Comparison	**Ventilation**	**Membrane**	**RBC**
Systematic Bias (Bland Altman Analysis)	−2 percentage points	−0.028	−0.013
Structural Similarity	0.52 (0.38 – 0.62)	0.71 (0.65 – 0.79)	0.14 (0.07 – 0.23)
PSNR	22.3 (20.2 – 24.3)	25.3 (24.7 – 26.3)	20.3 (17.7 – 22.5)

Comparison	**Normal Ventilation**	**Ventilation Defects**	**Normal Membrane**	**Low Membrane**	**Normal RBC**	**Low RBC**
Dice Coefficient	0.92 (0.88 – 0.94)	0.27 (0.02 – 0.69)	0.82 (0.73 – 0.90)	0.40 (0.09 – 0.59)	0.73 (0.58 – 0.80)	0.60 (0.54 – 0.69)
Average Distance	0.08 (0.05 – 0.13)	4.94 (0.52 – 14.01)	0.19 (0.10 – 0.29)	1.5 (0.6 – 4.49)	0.33 (0.24 – 0.55)	0.50 (0.39 – 0.60)